Check for updates

AGU ADVANCING EARTH AND SPACE SCIENCES

Geophysical Research Letters

RESEARCH LETTER
10.1029/2026GL126024

Accelerated Atmospheric Drying in Neighboring Rural Areas Across China Associated With Urban Warming

Xiaowen Huang[1], **Shuo Wang**[1,2], **Zhenzhong Zeng**[3,4,5], **Jinxin Zhu**[6], **and Dagang Wang**[6]

[1]State Key Laboratory of Climate Resilience for Coastal Cities, Department of Land Surveying and Geospatial Science, The Hong Kong Polytechnic University, Hong Kong, China, [2]Otto Poon Research Institute for Climate-Resilient Infrastructure and Research Institute for Land and Space, The Hong Kong Polytechnic University, Hong Kong, China, [3]School of Environmental Science and Engineering, Southern University of Science and Technology, Shenzhen, China, [4]State Key Laboratory of Soil Pollution Control and Safety, Southern University of Science and Technology, Shenzhen, China, [5]SUSTech Energy Institute for Carbon Neutrality, Southern University of Science and Technology, Shenzhen, China, [6]Carbon-Water Observation and Research Station in Karst Regions of Northern Guangdong, School of Geography and Planning, Sun Yat-Sen University, Guangzhou, China

Abstract Neighboring rural areas (i.e., rural zones surrounding cities) experience strong urban–rural interactions and provide critical ecosystem services, yet their responses to atmospheric drying remain poorly understood. Here, we quantify urban impacts on vapor pressure deficit (VPD) in neighboring rural areas across China by comparing station observations from neighboring rural stations (NRS) and remote rural stations (RRS, stations located in rural regions far from urban influence). During 1985–2019, 69% of cities exhibited faster VPD growth in their NRS than in their RRS, with a mean drying rate 27.5% higher than that of RRS. This disparity was more pronounced in summer, particularly within urban clusters. The NRS-RRS temperature difference dominated VPD variations, likely attributable to the urban-rural temperature gradient, whereby temperatures gradually decline outward from urban cores. These results reveal potential urban influence on rural atmospheric drying, highlighting ecosystem risks in neighboring rural areas and targeted adaptation needs in sustainable urban development.

Plain Language Summary Rural areas near cities play an important role in supporting ecosystems and influencing urban climate. While much attention has been paid to drying in cities, it remains unclear whether nearby rural areas are affected as well. In this study, we compared weather observations from rural areas near cities with those from rural areas farther away across China. We found that rural areas near cities have been drying 27.5% faster than more distant rural regions from 1985 to 2019. This effect is strongest during the summer and observed more frequently among megacities and cities within urban agglomerations. Faster drying is likely due to higher temperatures near cities. Heat from urban areas extends into nearby rural areas, creating a gradual decrease in temperature from cities to the countryside. This additional warming increases atmospheric dryness in nearby rural areas. These findings suggest growing risks to ecosystems and agriculture near cities and highlight the need for better planning to reduce the impacts of urban expansion.

Key Points:

- Rural areas near cities dry 27.5% faster than remote rural regions
- Rural drying is commonly observed around megacities, peaking during summer
- Urban-induced temperature gradients dominate the drying enhancement

Supporting Information:

Supporting Information may be found in the online version of this article.

Correspondence to:

S. Wang,
shuo.s.wang@polyu.edu.hk

Citation:

Huang, X., Wang, S., Zeng, Z., Zhu, J., & Wang, D. (2026). Accelerated atmospheric drying in neighboring rural areas across China associated with urban warming. *Geophysical Research Letters*, *53*, e2026GL126024. https://doi.org/10.1029/2026GL126024

Received 5 AUG 2026
Accepted 27 OCT 2026

Author Contributions:

Conceptualization: Shuo Wang
Data curation: Xiaowen Huang
Formal analysis: Xiaowen Huang
Funding acquisition: Shuo Wang
Methodology: Xiaowen Huang
Project administration: Shuo Wang
Resources: Shuo Wang
Software: Xiaowen Huang
Supervision: Shuo Wang
Validation: Xiaowen Huang, Shuo Wang, Zhenzhong Zeng, Jinxin Zhu, Dagang Wang
Visualization: Xiaowen Huang
Writing – original draft: Xiaowen Huang
Writing – review & editing: Shuo Wang, Zhenzhong Zeng, Jinxin Zhu, Dagang Wang

© 2026 The Author(s). Geophysical Research Letters published by Wiley Periodicals LLC on behalf of American Geophysical Union.
This is an open access article under the terms of the Creative Commons Attribution License, which permits use, distribution and reproduction in any medium, provided the original work is properly cited.

1. Introduction

Urban impervious surfaces drastically alter hydrological and thermal properties, reshaping local climate (Qian et al., 2022). Urban impacts may extend beyond city boundaries to neighboring rural areas. Lying close to built-up areas, these zones feature low impervious cover and dense vegetation, making them susceptible to urban disturbances, yet their climatic responses remain poorly characterized. Unlike remote rural areas that extend outward beyond the neighboring rural belt and lie farther from urban cores, city-adjacent rural areas maintain close socioeconomic connections with cities and perform critical urban climate regulation. Their agriculture promotes sustainable urban development by enabling short food supply chains in city food systems (FAO, Rikolto, & RUAF, 2022). Forests in surrounding rural areas are crucial for alleviating urban pollution (Baumgardner et al., 2012), reducing the intensity of urban heat island (UHI) (Yang et al., 2024), and mitigating flooding (Singh et al., 2024). Despite this indispensable role, prior research, even that referencing neighboring rural zones, has prioritized cities, with rural peripheries serving only as a backdrop in urban-focused analyses. Literature addressing rural areas has mostly focused on urbanization-driven land use (Clement et al., 2015; van Vliet

19448007, 2026, 21, Downloaded from https://agupubs.onlinelibrary.wiley.com/doi/10.1029/2026GL126024, Wiley Online Library on [06/11/2026]. See the Terms and Conditions (https://onlinelibrary.wiley.com/terms-and-conditions) on Wiley Online Library for rules of use; OA articles are governed by the applicable Creative Commons License

et al., 2017; S. Wang et al., 2021) and socioeconomic changes (Atmiş et al., 2007; Feng et al., 2019), yet few directly investigate their climatic responses to urban expansion.

Previous urban-focused studies have revealed urban modulation on local climates, including the UHI effect, urban canopy dynamics, and aerosol impacts on local circulation, boundary layer development, cloud formation, and evapotranspiration (Ding et al., 2025; Mazrooei et al., 2021; Shen & Yang, 2023; Vo et al., 2023; Zhang et al., 2017). These urban-driven climatic mechanisms can propagate into surrounding rural regions via land–atmosphere coupling, potentially extending beyond peri-urban zones (typically defined as the 10–20 km buffer zone extending from urban extents; Francini et al., 2024; Thebo et al., 2014). Sui et al. (2024) reported positive rainfall anomalies within cities and their downwind neighboring rural areas. Urban plume also transports pollutants downwind, exacerbating rural air pollution (Xu et al., 2011). However, how urbanization influences atmospheric dryness in neighboring rural areas, particularly in terms of vapor pressure deficit (VPD), remains largely unknown.

VPD integrates both atmospheric thermal and humidity conditions, and serves as a robust metric for atmospheric dryness in numerous studies (Yuan et al., 2025; Zhong et al., 2025). As a pivotal component of land–atmosphere coupling, VPD strongly modulates climate, ecosystems, and agriculture (Hsiao et al., 2019; S. Li et al., 2023; Massmann et al., 2019; Yuan et al., 2025). Rising VPD reduces plant stomatal conductance, thereby limiting photosynthesis and productivity (Grossiord et al., 2020; López et al., 2021). Existing work has focused on intra-urban VPD changes and the urban dry island (UDI) effect, where evapotranspiration acts as a primary regulator of urbanization-amplified atmospheric drying (Hao et al., 2023; Huang et al., 2022; Meili et al., 2022). Physically, VPD is controlled by air temperature and specific humidity. The well-documented UHI effect drives persistent and pronounced warming within urban regions, and this excess heat can diffuse into neighboring rural lands (Yang et al., 2024), which may alter local temperature and moisture in surrounding rural lands. Still, the magnitude and dominant pathways remain largely unquantified. Given dense vegetation in surrounding rural areas, it is equally important to examine whether urban expansion influences rural VPD variations and to uncover the potential urban-induced mechanisms.

China has undergone unprecedented urbanization with a coordinated development of large, medium, and small-sized cities (Sun et al., 2019). Since urban climatic impacts vary significantly with city size (Lu et al., 2024; B. Zhou et al., 2017), rural VPD responses to urbanization are unlikely to be uniform across cities of different sizes. However, existing studies on urban-induced VPD variation have largely been confined to metropolises (Gong et al., 2024; Huang et al., 2022; Lin et al., 2020; P. Wang et al., 2022), leaving the impacts of urbanization on surrounding rural areas at the national scale underexplored. Here, we quantify the effects of urban areas on VPD in neighboring rural areas across China using long-term meteorological observations. By comparing neighboring and remote rural sites, we (a) assess whether rural drying is enhanced near cities, (b) identify dominant drivers, and (c) explore their potential associations with urbanization.

2. Materials and Methods

2.1. Selection and Categorization of Weather Stations

We used daily climate data from 2,421 stations provided by the China Meteorological Administration to analyze rural VPD variations across China during 1985–2019. Stations were selected following WMO standards (WMO, 2017): a month was considered missing if it had ≥5 consecutive missing days or >11 total missing days; stations with >5 missing months over 35 years or a relocation distance >20 km were excluded, retaining 2,081 stations. Stations were classified into urban or rural based on the 30 m annual Global Impervious Surface Area (GISA) data set (Huang et al., 2021b). Its accuracy outperforms other existing 30 m ISA data sets, with an F-score of 0.954 (Huang et al., 2021b). Following Liao et al. (2018) and Su et al. (2025), a 2-km buffer was established around each station. For each year, stations with >33% impervious surface within the buffer were defined as urban stations, and those with <33% impervious surface were defined as rural stations.

Urban samples were selected from the Global Urban Boundary (GUB) data set (X. Li et al., 2020a). The data set provides urban boundaries and area data derived from the ISA data set for seven representative years (1990, 1995, 2000, 2005, 2010, 2015, and 2018) and has been widely applied in urban analysis (Su et al., 2025; Xiong et al., 2025). The 2018 GUB map was used to capture both old and newly developed urban areas of the study period (Yao et al., 2019). Since the climatic impacts of small cities are usually insufficient, only cities larger than

19448007, 2026, 21, Downloaded from https://agupubs.onlinelibrary.wiley.com/doi/10.1029/2026GL126024, Wiley Online Library on [06/11/2026]. See the Terms and Conditions (https://onlinelibrary.wiley.com/terms-and-conditions) on Wiley Online Library for rules of use; OA articles are governed by the applicable Creative Commons License

100 km^2 in 2018 were selected. To generate regular buffers around irregular urban boundaries, we first defined each city's minimum bounding urban polygon (U), which defines the urban region in this study (Figure S1 in Supporting Information S1). We then generated outward concentric rural buffers. Following Sui et al. (2024) and Xiong et al. (2025), the buffer radius r is calculated as:

$$r = \sqrt{\frac{S}{\pi}}, \tag{1}$$

where S denotes city area, assuming cities are circular. Concentric rural buffer rings were generated outward from the edge of the urban bounding polygon to form candidate neighboring and remote rural analysis zones.

We applied strict criteria for station selection. First, only stations that remained rural throughout the study period were retained to avoid impacts of rural-to-urban conversion. Second, any station functioning as a neighboring rural station (neighboring rural stations (NRS), rural stations located in urban region and neighboring rural areas) for one city and a remote rural station (remote rural stations (RRS), rural stations located in remote rural areas away from city) for another was classified as the NRS of the former city. Third, for each city, RRS with elevation differences exceeding 500 m from the NRS mean elevation were excluded to reduce topographical effects. Only cities with at least one NRS and one RRS after filtering were retained. We performed sensitivity tests to identify the optimal boundary separating neighboring and remote rural areas under these criteria. We ultimately selected the 5r buffer with a 2.5r dividing radius as the boundary between neighboring and remote rural areas, which maximized valid city samples. For each city, rural stations within 2.5r rural buffer were classified as NRS, and those within the 2.5–5r buffer were designated as RRS (Figure S1 in Supporting Information S1). This filtering yielded 36 cities for analysis. Following Su et al. (2025), cities were grouped by area percentiles: small (≤25th), medium (25th–50th), large (50th–75th), and mega (≥75th), with 9 cities in each group. We further analyzed four major urban agglomerations across China (Figure S2 in Supporting Information S1), including Beijing-Tianjin-Hebei (BTH), Central Plain Urban Agglomeration (CPUA), Yangtze-River-Delta (YRD), and Chengdu-Chongqing (CC). Agglomerations depend strongly on neighboring rural lands for climatic regulation and ecological services, making changes in rural dryness particularly relevant. The Pearl River Delta was excluded owing to only one eligible city.

2.2. VPD Calculation and Attribution

For each station, the monthly VPD (hPa) is derived from the daily air temperature T (°C) and relative humidity RH (%), as well as altitude (Z) following Yuan et al. (2019):

$$\mathrm{VPD} = \mathrm{SVP} - \mathrm{AVP}, \tag{2}$$

$$\mathrm{AVP} = \frac{\mathrm{RH}}{100} \times \mathrm{SVP}, \tag{3}$$

$$\mathrm{SVP} = 6.112 \times \left(1 + 7 \times 10^{-4} + 3.46 \times 10^{-6} p\right) \times \frac{17.67T}{e^{T+243.5}}, \tag{4}$$

where air pressure p is estimated from altitude ($p = p_{\mathrm{msl}} \left(\frac{(T+273.16)}{(T+273.16)+0.0065\times Z}\right)^{5.625}$, hPa) and p_{msl} represents mean sea level air pressure (1013.25 hPa). Annual and seasonal VPD values were then derived from monthly values. The VPD difference between NRS and RRS (ΔVPD) for each city was calculated as $\Delta\mathrm{VPD} = \mathrm{VPD}_{\mathrm{NRS}} - \mathrm{VPD}_{\mathrm{RRS}}$. The linear trends in ΔVPD were determined by least-squares regression, and significance was tested using the t-test.

We further performed an attribution analysis of annual ΔVPD using the methods described by Huang et al. (2022). Annual ΔVPD was attributed to the differences in air temperature (ΔT), specific humidity (Δq), and air pressure (Δp):

$$\Delta\mathrm{VPD} \approx \Delta\mathrm{SVP}(T) - \frac{p}{\varepsilon} \times \Delta q - \frac{q}{\varepsilon} \times \Delta p, \tag{5}$$

19448007, 2026, 21, Downloaded from https://agupubs.onlinelibrary.wiley.com/doi/10.1029/2026GL126024, Wiley Online Library on [06/11/2026]. See the Terms and Conditions (https://onlinelibrary.wiley.com/terms-and-conditions) on Wiley Online Library for rules of use; OA articles are governed by the applicable Creative Commons License

where ε is the ratio of the molar weight of water vapor and dry air ($\varepsilon = 0.622$). The plus and minus signs represent positive and negative contributions, respectively. The monthly specific humidity is calculated as:

$$q = \frac{\varepsilon \times \mathrm{AVP}}{p - 0.378 \times \mathrm{AVP}}. \quad (6)$$

2.3. Delineation of Urban–Rural Temperature Gradients

To investigate potential thermal interactions between urban and neighboring rural areas, we used the 1-km gridded monthly temperature data set across China from Peng et al. (2019). This data set was spatially downscaled from CRU and WorldClim data and has been validated against station observations. Urban and rural grids were distinguished using the GISA data set, with grids classified as urban if the impervious surface cover fraction exceeded 0.1 and as rural otherwise. The five concentric rural buffers (R1–R5) were further subdivided into 20 equal-width concentric rings, each with a radial width of r/4. For each city, we extracted only rural grids within the urban region (U) and each rural ring, and calculated their mean annual temperature and saturated vapor pressure (SVP). Rural grids located in remote rural that overlapped with the neighboring rural of other cities were excluded. For each city, temperature and SVP differences across U and all concentric rings were computed relative to the 2.5r concentric ring, which marks the boundary between neighboring and remote rural zones and served as the reference baseline. Convergent cross mapping (CCM), a method to separate causality from spurious correlation in nonlinear time series, was applied to identify causal links between U temperature and central neighboring rural SVP (Sugihara et al., 2012). Cross-mapping strength is quantified by the correlation coefficient (ρ) between predicted and observed values of the causal variable. Rising ρ with increasing time series and evident convergence signify a causal effect. We implemented CCM with *R* package multispatialCCM. The optimal embedding dimension was determined by simplex projection.

3. Results

3.1. Accelerated Drying in Neighboring Rural Areas

During 1985–2019, nearly all rural stations, including both NRS and RRS, exhibit increasing VPD trends, with the strongest significant signals were concentrated in central China (Figure S3 in Supporting Information S1). Across all rural stations, the mean VPD trend is 0.27 ± 0.04 hPa decade^{-1}. NRS experiences more rapid increases in VPD. In 69% of cities, drying rates are faster in adjacent rural areas than in their respective remote rural areas, and 65% of these cities show statistical significance (Figure 1a). Spatially, cities with a positive ΔVPD trend (defined as NRS VPD minus RRS VPD) are predominantly located in central, southwestern, and eastern China, while negative and non-significant trends are largely confined to western and southern parts of Central China. The national mean VPD trend for NRS is 0.30 ± 0.038 hPa decade^{-1}, 27.5% faster than that of RRS (0.24 ± 0.043 hPa decade^{-1}), resulting in a significant ($p < 0.01$) overall positive trend in ΔVPD of 0.066 ± 0.011 hPa decade^{-1} (Figure 1b). These findings are not sensitive to the radius thresholds used to define neighboring and remote rural zones. (Figure S4 in Supporting Information S1).

Across the four city-size categories, the number of cities with statistically significant increases in ΔVPD presents a clear size-dependent gradient: small cities have the fewest significant rising ΔVPD cases, while large and megacities have the most (Figure 1c). Boxplots further reveal the lowest median ΔVPD trend for small cities and the highest for megacities. For medium cities, despite a relatively high overall trend magnitude, the median trend is lower than that of megacities. This indicates that the overall distribution is skewed upward by a small subset of cities with strong positive trends. For large cities, despite matching megacities in the number of significant ΔVPD increases, they also contain more cities with significant declining trends, yielding overall higher trend variability. For urban agglomerations, all four major groups exhibit ΔVPD trends significantly above the national average. Specifically, the CPUA records the highest trend (0.16 ± 0.055 hPa decade^{-1}), followed by BTH (0.13 ± 0.026 hPa decade^{-1}) and CC (0.13 ± 0.029 hPa decade^{-1}), while YRD shows the lowest magnitude among the four (0.11 ± 0.032 hPa decade^{-1}; Figure 1d).

3.2. Enhanced Drying Peaks in Summer

The faster VPD rise of neighboring rural areas displays distinct seasonal patterns. This signal peaks in summer, with a mean ΔVPD trend of 0.16 ± 0.029 hPa decade^{-1}, nearly twice the annual mean trend (Figure 2a). Spring

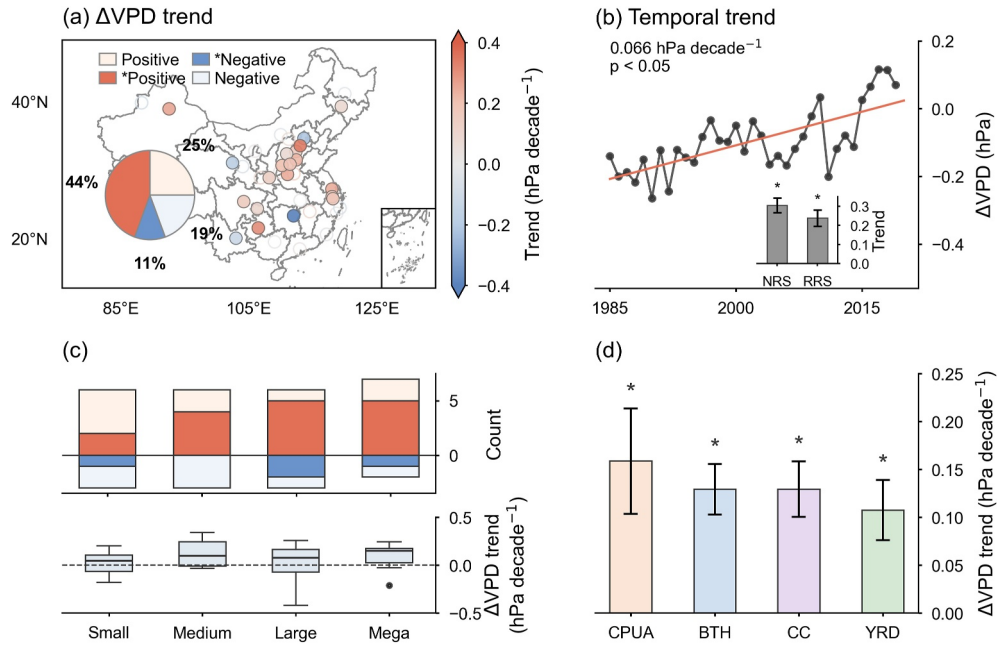


Figure 1. Spatiotemporal distribution of observed ΔVPD trends. (a) Spatial distribution of linear trends in rural ΔVPD (i.e., the VPD difference between neighboring rural stations (NRS) and remote rural stations (RRS), hPa decade^{-1}) across China. Solid circles indicate statistically significant trends ($p < 0.05$), while open circles represent non-significant trends. The inset pie chart summarizes the percentages of cities exhibiting non-significant positive, non-significant negative, significant positive, and significant negative trends, respectively. (b) Time series of the mean rural ΔVPD (hPa) across all cities in China. The bar plot shows the trend (hPa decade^{-1}) of the VPD series of all NRS and all RRS, respectively. The upper stacked bar plot of (c) displays the number of cities showing non-significant positive, non-significant negative, significant positive, and significant negative ΔVPD trends for small, medium, large, and megacities, respectively, with color consistent with (a). The lower boxplots present the distribution of ΔVPD trends across cities in each category, with the central line representing the median value. (d) Mean ΔVPD trend in four urban agglomerations, namely Central Plain Urban Agglomeration (CPUA), Beijing-Tianjin-Hebei (BTH), Chengdu-Chongqing (CC), and Yangtze-River-Delta (YRD). Error bars in the barplots indicate the standard error. Asterisks (*) indicate statistical significance at $p < 0.05$.

ranks second, with NRS drying faster than RRS at a rate of 0.070 ± 0.012 hPa decade^{-1} (Figure 2a). In autumn, the ΔVPD between neighboring and remote rural areas remains significant, though its magnitude falls below the annual average. Winter exhibits the weakest non-significant ΔVPD trend. The differences between seasonal ΔVPD trend and annual ΔVPD trend (ΔTrend) are then calculated. For summer, the season with the most pronounced rural drying signal, 72% of study cities show positive ΔTrend values, with the most prominent hotspots concentrated in central China (Figure 2b). This indicates that the enhanced neighboring rural drying in summer is a pervasive, widespread pattern. By contrast, such broad-scale intensification of rural drying is not observed in the other three seasons. Even in spring that shows the second-strongest drying signal, only 44% of cities show positive ΔTrend values, a proportion markedly lower than that in summer (Figure S5 in Supporting Information S1).

For the prevalence of positive ΔTrend, megacities contain the largest number of cities with enhanced summer drying relative to the annual baseline, followed by medium cities, while small cities have the fewest such cases (Figure 2c). Notably, the magnitude of ΔTrend does not follow the same size-dependent gradient. Medium cities record the highest median ΔTrend value, surpassing both large and megacities, whereas small cities exhibit the smallest overall change amplitude (Figure 2d). Although small cities exhibit relatively modest overall drying enhancement and rank lowest in summer ΔTrend, they record the strongest ΔTrend values among all four categories in spring, implying that small cities also feature distinct seasonal characteristics of neighboring rural drying response that cannot be overlooked (Figures S5b–S5c in Supporting Information S1).

For cities located in urban agglomeration, all four agglomerations exhibit substantial summer enhancement of the neighboring rural drying effect (Figure 2e). Except for the CC agglomeration, the summer ΔVPD trends of the other three agglomerations are more than double their corresponding annual mean values. In particular, the CPUA

19448007, 2026, 21, Downloaded from https://agupubs.onlinelibrary.wiley.com/doi/10.1029/2026GL126024, Wiley Online Library on [06/11/2026]. See the Terms and Conditions (https://onlinelibrary.wiley.com/terms-and-conditions) on Wiley Online Library for rules of use; OA articles are governed by the applicable Creative Commons License

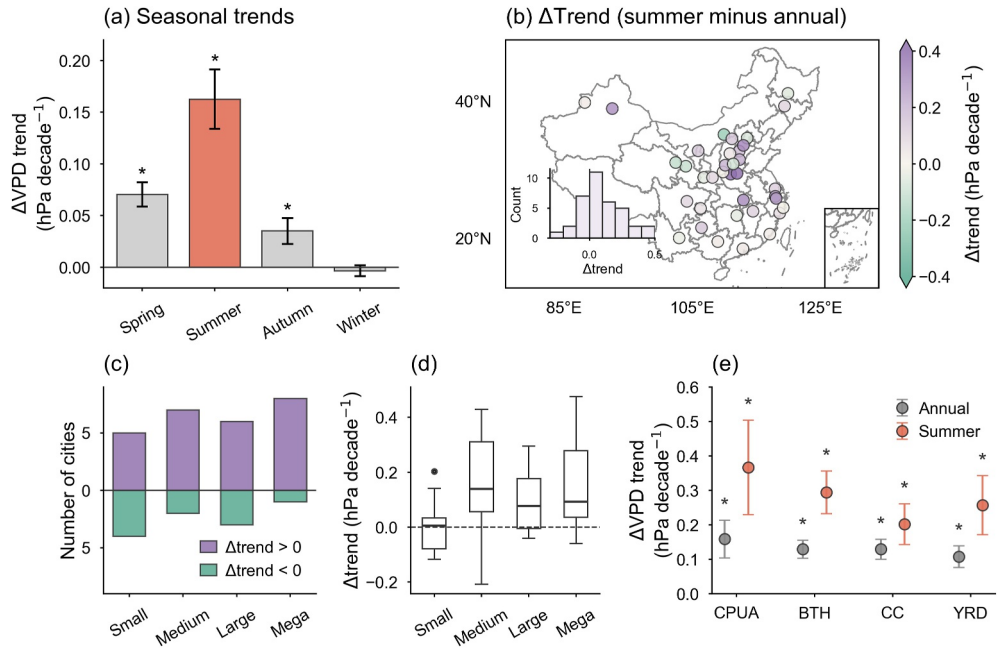


Figure 2. Enhanced summer ΔVPD trends. (a) Seasonal trends of ΔVPD across China. (b) Spatial distribution of summer-minus-annual trend difference (Δtrend). The inset histogram summarizes frequency distribution of Δtrend magnitudes. (c) Number of cities showing positive and negative Δtrend in each category, respectively. (d) The boxplot of Δtrend in each category, with the central line representing the median value. (e) Comparison of annual and summer ΔVPD trend of four urban agglomerations. The error bars represent the standard error. Asterisks (*) indicate statistical significance at $p < 0.05$.

and the YRD show the most prominent amplification, with summer ΔVPD trends reaching approximately 2.3 times their annual averages at 0.37 ± 0.14 hPa decade^{-1} and 0.26 ± 0.086 hPa decade^{-1}, respectively. These findings suggest that neighboring rural areas surrounding cities within urban agglomerations may face more extreme atmospheric drying conditions in summer, reflecting the amplified regional dryness risk associated with concentrated urban development.

3.3. Urban-Rural Temperature Gradient Dominates ΔVPD

Temperature differences dominate VPD variations between neighboring and remote rural areas. The temperature difference between NRS and RRS is identified as the dominant driver, with ΔVPD_T contributing 0.85 ± 0.031 of ΔVPD by elevating the SVP. Specific humidity differences (Δq) contribute 0.29 ± 0.027 of ΔVPD (Figure 3a), while the contribution of air pressure differences (Δp) is negligible. The relative contribution of ΔT and Δq to ΔVPD exhibits weak seasonal variability. ΔT contribution ranges from 67% in spring to 86% in winter. Δq exerts its maximum influence in spring, driving 33% of the VPD difference (Figure 3b). The spatial pattern of temperature-driven VPD changes, ΔVPD_T, is consistent with that of total ΔVPD, with most areas of central China showing a significant increase in ΔVPD_T (Figure 3c). In contrast, changes in the humidity-driven component, ΔVPD_q, are largely statistically insignificant across most regions, with the few significant changes concentrated in northwestern and central China (Figure 3d). Nevertheless, regional discrepancies in the dominant roles of ΔT and Δq are observed (Figure S6 in Supporting Information S1). Among cities with positive ΔVPD trends, megacities have the largest number of cities with statistically significant ΔVPD_T changes, reflecting the strong influence of temperature on VPD variations in the neighboring rural areas of megacities. Small and medium cities follow a consistent pattern, with more cities recording significant ΔVPD_T changes than significant ΔVPD_q changes. By contrast, large cities feature a higher count of significant ΔVPD_q changes, which indicates that humidity change can still exert an influence on regional VPD trends despite the dominant role of temperature.

Since NRS-RRS temperature differences dominate VPD changes, we further examined how UHI exacerbates dryness in NRAs through temperature-mediated effects using gridded data. Rural areas closer to urban cores generally exhibit higher temperatures than those farther from the city (Figure 4). The multi-year mean temperature of rural grids in the urban core (U) shows the highest warming in small and megacities, exceeding that of the

19448007, 2026, 21, Downloaded from https://agupubs.onlinelibrary.wiley.com/doi/10.1029/2026GL126024, Wiley Online Library on [06/11/2026]. See the Terms and Conditions (https://onlinelibrary.wiley.com/terms-and-conditions) on Wiley Online Library for rules of use; OA articles are governed by the applicable Creative Commons License

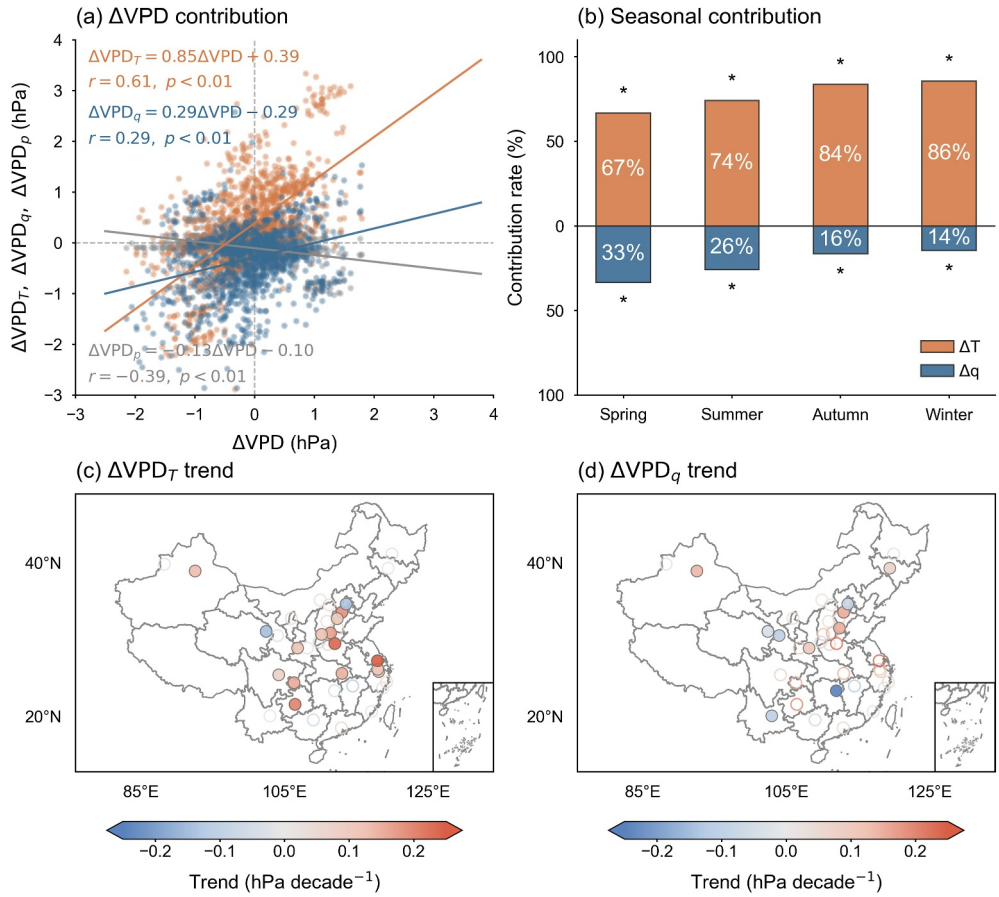


Figure 3. Contributions of temperature (ΔT), specific humidity (Δq), and air pressure (Δp) to annual and seasonal ΔVPD. (a) Decomposition of ΔVPD into temperature-driven (ΔVPD_T), humidity-driven (ΔVPD_q), and pressure-driven (ΔVPD_p) components. Blue, orange, and gray lines represent the corresponding regression lines, with statistical results shown in matching colors. (b) Relative contributions of ΔT, Δq to seasonal ΔVPD. Asterisks (*) indicate statistical significant regression slope of ΔVPD_T (ΔVPD_q) at $p < 0.05$. (c) and (d) depict spatial distributions of trends in ΔVPD_T and ΔVPD_q. Solid circles indicate statistically significant trends ($p < 0.05$), while open circles denote non-significant trends.

neighboring-remote rural boundary by 1.1°C and 1.3°C, respectively (Figures 4a and 4d). While UHI effect attenuates with increasing distance from urban cores, it persists in neighboring rural areas of all the cities. Medium cities show comparatively mild urban-rural temperature gradients (Figure 4b). In small, medium, and megacities, UHI-driven warming in neighboring rural areas elevates SVP, a key driver of VPD variation (Figures 4a and 4d). Specifically, U and R1 zones generally exhibit significantly faster increases in SVP in these cities. The urban core of megacities records the highest SVP trend, at 0.02 ± 0.0068 hPa decade^{-1} higher than the neighboring-remote rural boundary. Although both small and megacities experience considerable warming in their surrounding rural areas, megacities sustain a markedly larger difference in SVP trends between neighboring and remote rural zones, which leads to more prominent overall ΔVPD observed in megacities. CCM confirms causal links from U-zone temperature (U_T) to central neighboring rural ΔSVP ($\rho = 0.49$, $P < 0.01$), which is much higher than that from ΔSVP to U_T ($\rho = 0.23$, $P > 0.05$; Figure S7 in Supporting Information S1). This further demonstrates urban contribution to neighboring rural SVP through temperature modulation.

4. Discussion and Conclusions

Our results extend previous urban-focused studies (Gong et al., 2024; Huang et al., 2022; P. Wang et al., 2022) by showing that urban effects likely contribute to changes in atmospheric drying within neighboring rural areas. Rural regions adjacent to cities dry 27.5% faster than more remote areas. The faster drying in rural areas adjacent

19448007, 2026, 21, Downloaded from https://agupubs.onlinelibrary.wiley.com/doi/10.1029/2026GL126024, Wiley Online Library on [06/11/2026]. See the Terms and Conditions (https://onlinelibrary.wiley.com/terms-and-conditions) on Wiley Online Library for rules of use; OA articles are governed by the applicable Creative Commons License

10.1029/2026GL126024

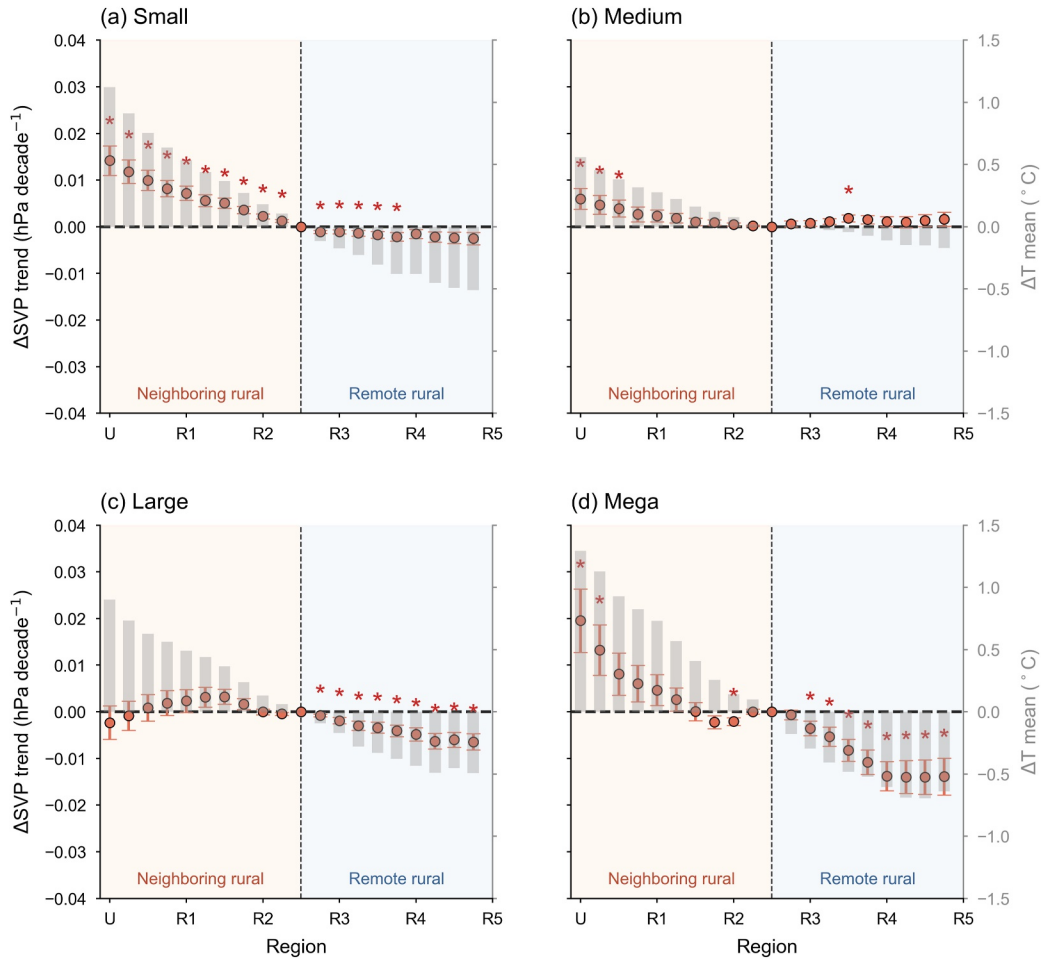


Figure 4. Rural temperature (T) and saturated vapor pressure (SVP) gradients from urban (U) to outer rural zones (R5) of (a) small, (b) medium, (c) large, and (d) mega-cities, respectively. Gray bars represent multi-year mean temperature differences (ΔT, 1985–2019) for rural grids in the U and inner 19 concentric rings relative to the ring at the 2.5r (boundary between neighboring and remote rural areas). Red error bars indicate the relative change in SVP trends for rural grids in the U and each concentric ring compared to the trends in the 2.5r ring. Points indicate the slope, error bars represent one standard error, and asterisks (*) denote statistical significance at $p < 0.05$.

to cities, particularly around megacities and within urban agglomerations, suggests a strong coupling between urban and rural climates (Moncada-Morales et al., 2025; Soto-Montes-de-Oca & Alfie-Cohen, 2019). The faster drying is most pronounced and widespread in summer, with the seasonal rate nearly double the annual average. This seasonal pattern aligns with documented urban drying seasonality, with rates considerably higher in spring and summer (Gong et al., 2024; Langendijk et al., 2019). Neighboring rural areas within major urban agglomerations exhibit particularly pronounced drying intensification across both the annual mean and summer, corroborating previous findings that large urban agglomerations experience a stronger urban amplification on atmospheric drying (P. Wang et al., 2022). This suggests a close connection between the drying of neighboring rural areas and urban cores.

Attribution analysis reveals temperature as the primary driver of ΔVPD, a pattern likely associated with the persistent urban-rural temperature gradient, indicating the spatial extension of the UHI effect into surrounding rural regions. Significant causal relationship from urban temperature to neighboring rural SVP is further detected. Adjacent rural areas experience higher temperatures than their remote counterparts, consistent with the dominant driver of urban atmospheric drying (Huang et al., 2022). Fan et al. (2017) found that the urban heat dome may extend 2–3 times the urban-core diameter, indicating widespread urban thermal influence on nearby rural areas.

19448007, 2026, 21, Downloaded from https://agupubs.onlinelibrary.wiley.com/doi/10.1029/2026GL126024, Wiley Online Library on [06/11/2026]. See the Terms and Conditions (https://onlinelibrary.wiley.com/terms-and-conditions) on Wiley Online Library for rules of use; OA articles are governed by the applicable Creative Commons License

19448007, 2026, 21, Downloaded from https://agupubs.onlinelibrary.wiley.com/doi/10.1029/2026GL126024, Wiley Online Library on [06/11/2026]. See the Terms and Conditions (https://onlinelibrary.wiley.com/terms-and-conditions) on Wiley Online Library for rules of use; OA articles are governed by the applicable Creative Commons License

The UHI effect typically peaks in summer (Schatz & Kucharik, 2014; D. Zhou et al., 2016a; B. Zhou et al., 2016b), a seasonal pattern that explains the pronounced summer peak in ΔVPD. Furthermore, although both small cities and megacities experience rising SVP in neighboring rural areas, the overall ΔVPD in small cities remains modest. Such divergence may be due to differences in their geographic settings. Megacities within urban agglomerations feature suppressed local evapotranspiration and reduced wind speed (Qian et al., 2022), restricting moisture transport and replenishment for neighboring rural within urban clusters, jointly elevating VPD. Rural areas surrounding small cities are generally located in less densely urbanized regions with sufficient moisture supply, which weakens net VPD amplification.

Nationally, humidity variations contribute only marginally to the overall ΔVPD variability, but still contribute to the VPD change at regional scales, for example, in large cities. This may involve UDI and urban moisture island (UMI) effects, whereby urban centers feature relatively lower or higher atmospheric humidity compared with surrounding rural areas. Intensive heat and moisture transport between urban cores and adjacent rural zones may enable UDI and UMI signals to substantially modulate humidity in neighboring rural areas of large cities. However, the occurrence and magnitude of UDI and UMI effects depend on multiple factors, including climatic backgrounds, urban morphological characteristics, and even seasonal and diurnal cycles. For example, UDI is pronounced in spring while UMI is stronger in summer for low-latitude cities, while mountainous cities facilitate humidity accumulation over urban areas (Huang & Song, 2023). Such spatiotemporal uncertainty complicates the quantification of urban-induced humidity modifications in neighboring rural regions, leaving the detailed physical mechanisms linking urban moisture to rural drying patterns to be further explored in future research.

Admittedly, this study has several limitations and uncertainties. First, strict rural station screening excluded sites with rural-to-urban transitions, limiting valid urban samples within many urban agglomerations, particularly those in southeastern China. This sample size constraint precludes robust generalized subgroup comparisons across climate regions, which could be improved by larger samples in future work. Second, our paired NRS-RRS analysis assumes identical large-scale atmospheric forcing in local scales, yet these two rural zones may still experience disparate climatic influences. To address this concern, we extracted variables from CMFD, GLEAM, and ERA5-Land data sets for NRS and RRS grids, calculated NRS-RRS differences per city and implemented XGBoost-SHAP modeling. Results reveal that temperature and specific humidity differences dominate ΔVPD, while other factors contribute only marginally (Figure S8 in Supporting Information S1). This reduces the likelihood that land-atmosphere coupling or regional climate shape ΔVPD through precipitation, evapotranspiration, and other variables. Nonetheless, we acknowledge that our analysis cannot fully disentangle temperature signals associated with urbanization from those driven by regional climate change. Third, our analysis terminates in 2019 owing to GUB temporal coverage. Nonetheless, the current 35-year study period sufficiently covers the rapid urbanization phase across China. Given projected UHI intensification (Liu et al., 2025), neighboring rural drying is likely to further intensify for recent years. Follow-up studies with extended, up-to-date data sets will enable more comprehensive investigations of such rural drying trends and further distinguish whether urban expansion or existing UHI variations dominate the formation of the rural temperature gradient.

These findings imply increasing risks to ecosystem functioning in rural areas that support urban systems. Enhanced rural drying may weaken vegetation cooling capacity by promoting stomatal closure and altering the regional surface energy balance, challenging sustainable urban development. Given the nonlinear amplification of drying driven by urban–rural temperature gradient and land–atmosphere coupling, rural drying may trigger cascading hydrological and ecological impacts. For example, rising summer VPD exacerbates soil moisture deficits (Chen et al., 2024), affecting water cycles and vegetation growth, while increasing the risk of extreme VPD events that damage agriculture and ecosystems (Hermann et al., 2024). These changes further erode the capacity of neighboring rural areas to buffer urban climate stress. Our findings, therefore, emphasize the urgent need for adaptive and precautionary measures to enhance climate resilience in neighboring rural areas and to support sustainable urban development, rather than focusing solely on urban centers.

Conflict of Interest

The authors declare no conflicts of interest relevant to this study.

Availability Statement

Relevant data of the study is stored at Zenodo (Huang, 2026). The observational meteorological data are provided by the CMA (2026). The GISA data set can be retrieved from Zenodo via Huang et al. (2021a). The GUB data set is available via X. Li et al. (2020b). The 1 km monthly temperature gridded data over China can be obtained from Peng (2019).

Acknowledgments
This study was supported by the Research Grants Council of the Hong Kong Special Administrative Region, China (Project PolyU/RGC 15232023) and the Otto Poon Research Institute for Climate-Resilient Infrastructure (Project P0055919).

References

Atmiş, E., Özden, S., & Lise, W. (2007). Urbanization pressures on the natural forests in Turkey: An overview. *Urban Forestry and Urban Greening*, *6*(2), 83–92. https://doi.org/10.1016/j.ufug.2007.01.002

Baumgardner, D., Varela, S., Escobedo, F. J., Chacalo, A., & Ochoa, C. (2012). The role of a peri-urban forest on air quality improvement in the Mexico City megalopolis. *Environmental Pollution*, *163*, 174–183. https://doi.org/10.1016/j.envpol.2011.12.016

Chen, X., Wang, J., Pan, F., Huang, B., Bi, P., Huang, N., et al. (2024). Summer atmospheric drying could contribute more to soil moisture change than spring vegetation greening. *npj Climate and Atmospheric Science*, *7*(1), 296. https://doi.org/10.1038/s41612-024-00844-6

Clement, M. T., Chi, G., & Ho, H. C. (2015). Urbanization and land-use change: A human ecology of deforestation across the United States, 2001–2006. *Sociological Inquiry*, *85*(4), 628–653. https://doi.org/10.1111/soin.12097

CMA. (2026). China surface meteorological observation data [Dataset]. Retrieved from https://data.cma.cn/en/?r=data/detail&dataCode=A.0012.0001

Ding, M., Zheng, X. T., Li, D., & Sun, T. (2025). Background wind speeds outweigh urban heat islands in downwind precipitation enhancement by cities. *Geophysical Research Letters*, *52*(12), e2024GL114142. https://doi.org/10.1029/2024GL114142

Fan, Y., Li, Y., Bejan, A., Wang, Y., & Yang, X. (2017). Horizontal extent of the urban heat dome flow. *Scientific Reports*, *7*(1), 11681. https://doi.org/10.1038/s41598-017-09917-4

FAO, Rikolto, & RUAF. (2022). Urban and peri-urban agriculture sourcebook—from production to food systems. *Rome, FAO and Rikolto*. https://doi.org/10.4060/cb9722en

Feng, W., Liu, Y., & Qu, L. (2019). Effect of land-centered urbanization on rural development: A regional analysis in China. *Land Use Policy*, *87*, 104072. https://doi.org/10.1016/j.landusepol.2019.104072

Francini, S., Chirici, G., Chiesi, L., Costa, P., Caldarelli, G., & Mancuso, S. (2024). Global spatial assessment of potential for new peri-urban forests to combat climate change. *Nature Cities*, *1*(4), 286–294. https://doi.org/10.1038/s44284-024-00049-1

Gong, S., She, D., Xia, J., & Wang, T. (2024). Impacts of urbanization on urban-rural VPD disparities across different subregions in China: A quantitative analysis based on station-pairing and partial differential methods. *Atmospheric Research*, *311*, 107681. https://doi.org/10.1016/j.atmosres.2024.107681

Grossiord, C., Buckley, T. N., Cernusak, L. A., Novick, K. A., Poulter, B., Siegwolf, R. T., et al. (2020). Plant responses to rising vapor pressure deficit. *New Phytologist*, *226*(6), 1550–1566. https://doi.org/10.1111/nph.16485

Hao, L., Sun, G., Huang, X., Tang, R., Jin, K., Lai, Y., et al. (2023). Urbanization alters atmospheric dryness through land evapotranspiration. *npj Climate and Atmospheric Science*, *6*(1), 149. https://doi.org/10.1038/s41612-023-00479-z

Hermann, M., Wernli, H., & Röthlisberger, M. (2024). Drastic increase in the magnitude of very rare summer-mean vapor pressure deficit extremes. *Nature Communications*, *15*(1), 7022. https://doi.org/10.1038/s41467-024-51305-w

Hsiao, J., Swann, A. L., & Kim, S. H. (2019). Maize yield under a changing climate: The hidden role of vapor pressure deficit. *Agricultural and Forest Meteorology*, *279*, 107692. https://doi.org/10.1016/j.agrformet.2019.107692

Huang, X. (2026). Accelerated atmospheric drying in neighboring rural areas across China associated with urban warming [Dataset]. *Zenodo*. https://doi.org/10.5281/zenodo.22896705

Huang, X., Hao, L., Sun, G., Yang, Z. L., Li, W., & Chen, D. (2022). Urbanization aggravates effects of global warming on local atmospheric drying. *Geophysical Research Letters*, *49*(2), e2021GL095709. https://doi.org/10.1029/2021GL095709

Huang, X., Li, J., Yang, J., Zhang, Z., Li, D., & Liu, X. (2021a). 30 m global impervious surface area dynamics and urban expansion pattern observed by Landsat satellites: From 1972 to 2019 [Dataset]. *Zenodo*. https://doi.org/10.5281/zenodo.5136330

Huang, X., Li, J., Yang, J., Zhang, Z., Li, D., & Liu, X. (2021b). 30 m global impervious surface area dynamics and urban expansion pattern observed by Landsat satellites: From 1972 to 2019. *Science China Earth Sciences*, *64*(11), 1922–1933. https://doi.org/10.1007/s11430-020-9797-9

Huang, X., & Song, J. (2023). Urban moisture and dry islands: Spatiotemporal variation patterns and mechanisms of urban air humidity changes across the globe. *Environmental Research Letters*, *18*(10), 103003. https://doi.org/10.1088/1748-9326/acf7d7

Langendijk, G. S., Rechid, D., & Jacob, D. (2019). Urban areas and urban–rural contrasts under climate change: What does the EURO-CORDEX ensemble tell us? Investigating near surface humidity in Berlin and its surroundings. *Atmosphere*, *10*(12), 730. https://doi.org/10.3390/atmos10120730

Li, S., Wang, G., Chai, Y., Miao, L., Hagan, D. F. T., Sun, S., et al. (2023). Increasing vapor pressure deficit accelerates land drying. *Journal of Hydrology*, *625*, 130062. https://doi.org/10.1016/j.jhydrol.2023.130062

Li, X., Gong, P., Zhou, Y., Wang, J., Bai, Y., Chen, B., et al. (2020a). Mapping global urban boundaries from the global artificial impervious area (GAIA) data. *Environmental Research Letters*, *15*(9), 094044. https://doi.org/10.1088/1748-9326/ab9be3

Li, X., Gong, P., Zhou, Y., Wang, J., Bai, Y., Chen, B., et al. (2020b). Mapping global urban boundaries from the global artificial impervious area (GAIA) data [Dataset]. https://data-starcloud.pcl.ac.cn/iearthdata/14

Liao, W., Liu, X., Li, D., Luo, M., Wang, D., Wang, S., et al. (2018). Stronger contributions of urbanization to heat wave trends in wet climates. *Geophysical Research Letters*, *45*(20), 11–310. https://doi.org/10.1029/2018GL079679

Lin, L., Chan, T. O., Ge, E., Wang, X., Zhao, Y., Yang, Y., et al. (2020). Effects of urban land expansion on decreasing atmospheric moisture in Guangdong, South China. *Urban Climate*, *32*, 100626. https://doi.org/10.1016/j.uclim.2020.100626

Liu, Z., Li, J., Wu, Y., Qin, C., & Liu, Y. (2025). Temporal trend of the frequency and maximum durations of surface urban heat islands over global cities. *Sustainable Cities and Society*, *120*, 106141. https://doi.org/10.1016/j.scs.2025.106141

López, J., Way, D. A., & Sadok, W. (2021). Systemic effects of rising atmospheric vapor pressure deficit on plant physiology and productivity. *Global Change Biology*, *27*(9), 1704–1720. https://doi.org/10.1111/gcb.15548

Lu, Y., Yu, Z., Albertson, J. D., Chen, H., Hu, L., Pendergrass, A., et al. (2024). Understanding the influence of urban form on the spatial pattern of precipitation. *Earth's Future*, *12*(1), e2023EF003846. https://doi.org/10.1029/2023EF003846

19448007, 2026, 21, Downloaded from https://agupubs.onlinelibrary.wiley.com/doi/10.1029/2026GL126024, Wiley Online Library on [06/11/2026]. See the Terms and Conditions (https://onlinelibrary.wiley.com/terms-and-conditions) on Wiley Online Library for rules of use; OA articles are governed by the applicable Creative Commons License

Massmann, A., Gentine, P., & Lin, C. (2019). When does vapor pressure deficit drive or reduce evapotranspiration? *Journal of Advances in Modeling Earth Systems*, *11*(10), 3305–3320. https://doi.org/10.1029/2019MS001790

Mazrooei, A., Reitz, M., Wang, D., & Sankarasubramanian, A. (2021). Urbanization impacts on evapotranspiration across various spatio-temporal scales. *Earth's Future*, *9*(8), e2021EF002045. https://doi.org/10.1029/2021EF002045

Meili, N., Paschalis, A., Manoli, G., & Fatichi, S. (2022). Diurnal and seasonal patterns of global urban dry islands. *Environmental Research Letters*, *17*(5), 054044. https://doi.org/10.1088/1748-9326/ac68f8

Moncada-Morales, G. A., Livesley, S. J., Nice, K. A., Pianella, A., & Carpio, M. (2025). Intense drought and vegetation browning exacerbate air temperature rise in unirrigated peri-urban areas under global warming. *Sustainable Cities and Society*, *130*, 106643. https://doi.org/10.1016/j.scs.2025.106643

Peng, S. (2019). 1-km monthly mean temperature dataset for China (1901-2025) [Dataset]. *National Tibetan Plateau / Third Pole Environment Data Center*. https://doi.org/10.11888/Meteoro.tpdc.270961

Peng, S., Ding, Y., Liu, W., & Li, Z. (2019). 1 km monthly temperature and precipitation dataset for China from 1901 to 2017. *Earth System Science Data*, *11*(4), 1931–1946. https://doi.org/10.5194/essd-11-1931-2019

Qian, Y., Chakraborty, T. C., Li, J., Li, D., He, C., Sarangi, C., et al. (2022). Urbanization impact on regional climate and extreme weather: Current understanding, uncertainties, and future research directions. *Advances in Atmospheric Sciences*, *39*(6), 819–860. https://doi.org/10.1007/s00376-021-1371-9

Schatz, J., & Kucharik, C. J. (2014). Seasonality of the urban heat island effect in Madison, Wisconsin. *Journal of Applied Meteorology and Climatology*, *53*(10), 2371–2386. https://doi.org/10.1175/JAMC-D-14-0107.1

Shen, Y., & Yang, L. (2023). Divergent urban signatures in rainfall anomalies explained by pre-storm environment contrast. *Geophysical Research Letters*, *50*(5), e2022GL101658. https://doi.org/10.1029/2022GL101658

Singh, R., Chavan, S. B., Kakade, V. D., Morade, A. S., Singh, A. K., Rawale, G. B., et al. (2024). Ecosystem services provided by urban and peri-urban forests. In *Urban forests, climate change and environmental pollution: Physio-biochemical and molecular perspectives to enhance urban resilience* (pp. 417–445). Springer Nature Switzerland.

Soto-Montes-de-Oca, G., & Alfie-Cohen, M. (2019). Impact of climate change in Mexican peri-urban areas with risk of drought. *Journal of Arid Environments*, *162*, 74–88. https://doi.org/10.1016/j.jaridenv.2018.10.006

Su, J., Miao, C., Hu, J., Wu, Y., & Ji, J. (2025). Widening urban–rural precipitation differences in China: Regionally varied intensification since 2000. *Earth's Future*, *13*(9), e2025EF006657. https://doi.org/10.1029/2025EF006657

Sugihara, G., May, R., Ye, H., Hsieh, C. H., Deyle, E., Fogarty, M., & Munch, S. (2012). Detecting causality in complex ecosystems. *Science*, *338*(6106), 496–500. https://doi.org/10.1126/science.1227079

Sui, X., Yang, Z. L., Shepherd, M., & Niyogi, D. (2024). Global scale assessment of urban precipitation anomalies. *Proceedings of the National Academy of Sciences*, *121*(38), e2311496121. https://doi.org/10.1073/pnas.2311496121

Sun, B., Jin, X., & Lin, J. (2019). China's new pattern of urbanization toward coordinated development of large, medium and small cities: Evolution and determinants of city size distribution since 1952. *Geographical Research*, *38*(1), 75–84. https://doi.org/10.11821/dlyj020180443

Thebo, A. L., Drechsel, P., & Lambin, E. F. (2014). Global assessment of urban and peri-urban agriculture: Irrigated and rainfed croplands. *Environmental Research Letters*, *9*(11), 114002. https://doi.org/10.1088/1748-9326/9/11/114002

van Vliet, J., Eitelberg, D. A., & Verburg, P. H. (2017). A global analysis of land take in cropland areas and production displacement from urbanization. *Global Environmental Change*, *43*, 107–115. https://doi.org/10.1016/j.gloenvcha.2017.02.001

Vo, T. T., Hu, L., Xue, L., Li, Q., & Chen, S. (2023). Urban effects on local cloud patterns. *Proceedings of the National Academy of Sciences*, *120*(21), e2216765120. https://doi.org/10.1073/pnas.2216765120

Wang, P., Tong, X., Qiu, J., Chen, Y., Wu, S., Chan, T. O., et al. (2022). Amplification effect of urbanization on atmospheric aridity over China under past global warming. *Earth's Future*, *10*(5), e2021EF002335. https://doi.org/10.1029/2021EF002335

Wang, S., Bai, X., Zhang, X., Reis, S., Chen, D., Xu, J., & Gu, B. (2021). Urbanization can benefit agricultural production with large-scale farming in China. *Nature Food*, *2*(3), 183–191. https://doi.org/10.1038/s43016-021-00228-6

World Meteorological Organization (WMO). (2017). Guidelines on the calculation of climate normals (WMO-No. 1203). Retrieved from https://library.wmo.int/index.php?lvl=notice_display&id=20130

Xiong, J., Yang, Y., Yang, L., & Yang, D. (2025). Asymmetric shifts in precipitation due to urbanization across global cities. *Nature Communications*, *16*(1), 5802. https://doi.org/10.1038/s41467-025-61053-0

Xu, J., Ma, J. Z., Zhang, X. L., Xu, X. B., Xu, X. F., Lin, W. L., et al. (2011). Measurements of ozone and its precursors in Beijing during summertime: Impact of urban plumes on ozone pollution in downwind rural areas. *Atmospheric Chemistry and Physics*, *11*(23), 12241–12252. https://doi.org/10.5194/acp-11-12241-2011

Yang, M., Ren, C., Wang, H., Wang, J., Feng, Z., Kumar, P., et al. (2024). Mitigating urban heat island through neighboring rural land cover. *Nature Cities*, *1*(8), 522–532. https://doi.org/10.1038/s44284-024-00091-z

Yao, R., Wang, L., Huang, X., Gong, W., & Xia, X. (2019). Greening in rural areas increases the surface urban heat island intensity. *Geophysical Research Letters*, *46*(4), 2204–2212. https://doi.org/10.1029/2018GL081816

Yuan, W., Tian, J., Wang, M., Wang, S., Xu, W., Wang, Y., et al. (2025). Impacts of rising atmospheric dryness on terrestrial ecosystem carbon cycle. *Nature Reviews Earth & Environment*, *6*(11), 1–16. https://doi.org/10.1038/s43017-025-00726-2

Yuan, W., Zheng, Y., Piao, S., Ciais, P., Lombardozzi, D., Wang, Y., et al. (2019). Increased atmospheric vapor pressure deficit reduces global vegetation growth. *Science Advances*, *5*(8), eaax1396. https://doi.org/10.1126/sciadv.aax1396

Zhang, Y., Miao, S., Dai, Y., & Bornstein, R. (2017). Numerical simulation of urban land surface effects on summer convective rainfall under different UHI intensity in Beijing. *Journal of Geophysical Research: Atmospheres*, *122*(15), 7851–7868. https://doi.org/10.1002/2017JD026614

Zhong, Z., Chen, H. W., Dai, A., Zhou, T., He, B., & Su, B. (2025). Sub-diurnal asymmetric warming has amplified atmospheric dryness since the 1980s. *Nature Communications*, *16*(1), 8247. https://doi.org/10.1038/s41467-025-63672-z

Zhou, B., Lauwaet, D., Hooyberghs, H., De Ridder, K., Kropp, J. P., & Rybski, D. (2016). Assessing seasonality in the surface urban heat island of London. *Journal of Applied Meteorology and Climatology*, *55*(3), 493–505. https://doi.org/10.1175/JAMC-D-15-0041.1

Zhou, B., Rybski, D., & Kropp, J. P. (2017). The role of city size and urban form in the surface urban heat island. *Scientific Reports*, *7*(1), 4791. https://doi.org/10.1038/s41598-017-04242-2

Zhou, D., Zhang, L., Hao, L., Sun, G., Liu, Y., & Zhu, C. (2016). Spatiotemporal trends of urban heat island effect along the urban development intensity gradient in China. *Science of the Total Environment*, *544*, 617–626. https://doi.org/10.1016/j.scitotenv.2015.11.168

19448007, 2026, 21, Downloaded from https://agupubs.onlinelibrary.wiley.com/doi/10.1029/2026GL126024, Wiley Online Library on [06/11/2026]. See the Terms and Conditions (https://onlinelibrary.wiley.com/terms-and-conditions) on Wiley Online Library for rules of use; OA articles are governed by the applicable Creative Commons License